NACA RM E53F23

NACA



# RESEARCH MEMORANDUM

## INVESTIGATION OF A SUPERSONIC-COMPRESSOR ROTOR WITH TURNING TO AXIAL DIRECTION

## I - ROTOR DESIGN AND PERFORMANCE

By Edward R. Tysl, John F. Klapproth, and Melvin J. Hartmann

Lewis Flight Propulsion Laboratory
Cleveland, Ohio





NATIONAL ADVISORY COMMITTEE
FOR AERONAUTICS

WASHINGTON

August 19, 1953

NATIONAL ADVISORY COMMITTEE FOR AERONAUTICS

RESEARCH MEMORANDUM

# INVESTIGATION OF A SUPERSONIC-COMPRESSOR ROTOR WITH TURNING TO AXIAL DIRECTION

## I - ROTOR DESIGN AND PERFORMANCE

By Edward R. Tysl, John F. Klapproth, and Melvin J. Hartmann



## SUMMARY

An approximate, quasi-three-dimensional design procedure has been adapted to the design of high solidity, impulse-type supersonic compressors. The principle of zero absolute circulation for flows with no losses was used to determine the blade-surface velocities. The stream-filament approach with the assumption of axisymmetric flow was used to obtain the streamline configuration in the hub-to-shroud plane.

The method was applied to a compressor rotor having a tip speed of 1600 feet per second in air, an inlet hub-tip radius ratio of 0.75, and an axial discharge relative to the rotor. The design pressure ratio at the mean radius for isentropic flow was 6.9 with an absolute discharge Mach number of 2.03. When tested in Freon-12 at an equivalent speed of 97.5 percent of design and open-throttle condition, the rotor obtained a total-pressure ratio of 5.7 at an adiabatic efficiency of about 0.89. The absolute mean-radius discharge Mach number was 1.93. At other than design speed, the level of adiabatic efficiency remained high. Appreciable discrepancies between the measured and isentropically predicted discharge values existed at the rotor tip because of the losses occurring in this region.

## INTRODUCTION

Impulse-type supersonic-compressor rotors are designed for a large turning in the rotor blade passage with only a low or moderate static-pressure rise across the rotor. The flow enters the diffusing stators with supersonic velocities and is decelerated to subsonic velocities, and kinetic energy imparted by the rotor is converted into static pressure.

Several impulse-type supersonic compressors were experimentally investigated and reported in references 1 to 3. The compressor rotors of these investigations obtained total-pressure ratios of 3.6 and 6.6

at adiabatic efficiencies of 0.80 and 0.78, respectively. Although these performance values seem reasonable for a rotor component, when attempts were made to recover the large velocity pressure by use of diffusing stators installed behind these rotors, poor stage performance was obtained (refs. 2 and 4). For stator-entrance Mach numbers above 1.4, substantial losses in total pressure were observed across the stators. The data of reference 4 indicate that the poor flow conditions leaving the rotor probably contribute appreciably to the large total-pressure drop, as might be expected from experience with centrifugal diffusers. Consequently, even though the stators seem to represent the major problem, considerable improvement may be gained in stage performance by improving stator-entrance conditions through increasing compressor rotor efficiency.

In the present study, conducted at the NACA Lewis laboratory, an attempt was made to improve the rotor efficiency in an effort to alleviate the stator problem as much as possible. The approach to the rotor design was to hold the velocity peaks on the rotor blade suction surface to a minimum, with the required diffusion (or velocity ratio from $V_{max}$ to $V_{min}$) on the blade surface restricted to very moderate values compared with usual subsonic limits. An approximate design method based on a quasi-three-dimensional approach, as suggested in reference 5, was applied to determine the passage geometry and the estimated blade-surface velocities. The limiting diffusion was selected to be appreciably less than that proposed for incompressible flow in reference 6, where an attempt was made to obtain maximum circulation without flow separation.

The rotor design method and the performance of the rotor as a separate component are considered in this report.

## ROTOR DESIGN METHOD

### General Considerations

Pressure ratios up to 6.5 can be theoretically obtained with nearly axial discharge relative to the rotor with rotor tip speeds of 1600 feet per second (ref. 7). A large variation in the width of the flow channel between blades results, however, when turning from the relative rotor-entrance angle to near the axial direction. Since the rotor is designed for nearly the same relative Mach number at entrance and exit, the increased channel width resulting from the turning must be taken up with a radial contraction of the channel height in passing through the rotor. This radial contraction of the streamlines prohibits the design of the rotor blade profile with the usual two-dimensional method of characteristics.

Considerations of the stresses resulting from the high rotational speeds indicate the desirability of having radial blade elements with either a constant blade thickness radially or a radial taper. These restrictions on radial blade elements and thickness distribution leave the determination of the blade mean line and thickness free along only one annular stream tube. Since the flow conditions at the rotor tip appear to be most severe, the limiting surface gradients were selected along the tip streamline. The tip blade shape computed from the prescribed conditions for the tip streamline then determines the blade shape and thickness distribution for all other stream surfaces. The hub shape required to satisfy the desired mean flow conditions at the tip is determined by computing through the rotor successive streamlines an incremental distance apart. The computation is continued for successively lower streamlines, until either the desired weight flow or entrance hub-tip radius ratio is obtained.

## Determination of Rotor Tip Blade Section

Coordinate system. - A typical impulse-type supersonic compressor may be represented by figure 1. The coordinate system of $R,\theta,z$ is alined with the z-axis along the axis of rotation and $\theta$ positive in the direction of rotation. The system is considered fixed relative to the rotor. The coordinates $R$ and $z$ and all linear dimensions have been made dimensionless by dividing by the rotor tip radius.

The quasi-three-dimensional approach to the rotor design is similar to that used in reference 5. In order to investigate the blade-to-blade variations, the assumption is made that an entering stream tube enclosed by the leading edges of two adjacent blades and an incremental annular height $\Delta R$ will be bounded by surfaces of revolution obtained by rotating the meridional streamlines. By choosing a sufficiently small annular height, the flow conditions can be assumed constant normal to the flow path, and the problem reduces to one of two-dimensional flow between blades.

Continuity along stream surface. - The continuity equation for the flow through the incremental annulus can be expressed as

$$\frac{2\pi R_1 \rho_1 Q_1 \cos \beta_1'}{n\sqrt{1 + \cos^2\beta_1' \tan^2\varphi_1}} = \int_{\theta_p}^{\theta_s} \frac{\rho Q \cos \beta' \, Rh \, d\theta}{\sqrt{1 + \cos^2\beta' \tan^2\varphi}} \qquad (1)$$

where $R(\theta_p-\theta_s)$ represents the distance between pressure and suction surfaces of the blade, and the subscript 1 represents conditions at the rotor inlet. Other symbols are defined in the appendix.

For relatively thin rotor blades of high solidity, the flow angle $\beta'$ may be considered constant across the passage. Furthermore, since it has been assumed that the flow lies on a surface of revolution, R, h, and $\varphi$ will remain constant from $\theta_p$ to $\theta_s$. Then, equation (1) can be written as

$$\frac{R_1\rho_1Q_1\cos\beta_1'}{\sqrt{1+\cos^2\beta_1'\tan^2\varphi_1}} = \frac{R\rho_mQ_mh\cos\beta'}{\sqrt{1+\cos^2\beta'\tan^2\varphi}}\left(1-\frac{nt}{2\pi R}\right) \qquad (2)$$

where

$$\rho_mQ_m = \frac{\int_{\theta_p}^{\theta_s}\rho Q\,d\theta}{\theta_s-\theta_p}$$

and the subscript m represents mean conditions of density and velocity across the channel. The further assumption, that the mean velocity and density will occur on the mean streamline, will be exact only in the case of an infinite solidity.

Energy. - The relation between density ratio and the dimensionless relative velocity is expressed by

$$\rho = \left[1+\frac{\gamma-1}{2}\left(M_t^2R^2-Q^2-2M_tRV_{\theta,1}\right)\right]^{\frac{1}{\gamma-1}} = p^{\frac{1}{\gamma}} \qquad (3)$$

Specified conditions. - From the design vector diagram, the tip inlet and outlet velocity ratios are known. A smooth variation of $Q_m$ may be specified from the rotor entrance to the rotor exit in order to provide a uniform distribution of static pressure along the outer casing. From continuity (eq. (2)), the inlet and outlet h ratios may be determined, with an arbitrary wake allowance specified for $nt/2\pi R$ at the rotor exit. Since a smooth hub shape is desirable, a uniform variation in h through the rotor may be specified.

The rate of increase of the absolute tangential velocity through the rotor will reflect the velocity difference on the blade surfaces.

Consequently, a specified uniform increase in the absolute tangential velocity should provide a reasonable velocity distribution on the blade surface. After specifying the mean velocity and absolute tangential velocity distribution, the mean flow angle $\beta'$ may be computed. With the prescribed h ratio, the resultant thickness distribution $nt/2\pi R$ may then be computed from equations (2) and (3). (The distribution of R and $\varphi$ is known from the tip streamline or outer shroud shape.) If the resultant mean flow angle or thickness distribution is not satisfactory (i.e., negative blade thickness), slight adjustments in $Q_m$, h, or $V_\theta$ may be made to improve the distribution. A different selection of specified conditions other than those listed above could, of course, be made to suit the particular problem.

Blade-surface velocities. - Once the mean flow conditions and the blade shape have been determined, then an approximate solution for the blade-surface velocities is desirable in order to check the velocity distribution resulting from the specified mean relative velocity and absolute tangential velocity distributions. In addition, the number of blades n may then be selected in order that the ratio of the maximum velocity on the suction surface to the minimum or exit velocity on that surface be held within specified limits.

The blade-to-blade solution is obtained by applying the method of reference 8. Consider the elemental area bounded by the pressure and suction surfaces of the blades and two lines of constant z an infinitesimal distance $\Delta s$ apart (fig. 1). If it is assumed that there are no entropy gradients, the absolute circulation around the fluid strip is zero. Then, as $\Delta z$ approaches zero,

$$-\frac{Q_s(1+\cos^2\beta_s' \tan^2\varphi)^{\frac{1}{2}}}{\cos\beta_s'}+\frac{Q_p(1+\cos^2\beta_p' \tan^2\varphi)^{\frac{1}{2}}}{\cos\beta_p'}+M_tR(\tan\beta_p'-\tan\beta_s')+$$

$$\frac{d}{dz}\int_{\theta_p}^{\theta_s}\left[\frac{Q\sin\beta'}{(1+\cos^2\beta'\tan^2\varphi)^{\frac{1}{2}}}+M_tR\right]R\,d\theta=0 \qquad (4)$$

If it is assumed, as in the case of the continuity equation, that $\beta_s' \approx \beta_p' \approx \beta_m'$, then

$$n(Q_s - Q_p) \approx \frac{2\pi \cos \beta}{(1 + \cos^2\beta' \tan^2 \varphi)^{\frac{1}{2}}} \times$$

$$\frac{d}{dz}\left[\frac{Q_m \sin \beta'}{(1 + \cos^2\beta' \tan^2 \varphi)^{\frac{1}{2}}} + M_t R\right] R\left(1 - \frac{nt}{2\pi R}\right) \qquad (5)$$



From the previously specified conditions, equation (5) can be solved for $n(Q_s - Q_p)$. If the further assumption is made that $Q$ varies linearly across the passage, then

$$Q_m = \frac{1}{2}(Q_s + Q_p) \qquad (6)$$

For any given number of blades, the surface velocity distributions may be obtained from equations (5) and (6) in the form

$$Q_s \approx Q_m + \frac{1}{2}(Q_s - Q_p) \qquad (6a)$$

$$Q_p \approx Q_m - \frac{1}{2}(Q_s - Q_p) \qquad (6b)$$

If the resulting approximate values of blade-surface velocity ratios show unnecessary peaks, the absolute tangential velocity distribution can be modified to obtain a more desirable distribution.

## Tip-to-Hub Solution

The previous section provided a blade shape and thickness distribution at the tip streamline resulting from specified conditions on the annular height of the stream tube $h$ as well as on the mean relative velocity and absolute tangential velocity distributions. The necessary hub shape required to give the desired $h$ distribution on the tip streamline must now be determined.

The mean flow surface throughout the passage is determined by passing radial elements through the tip mean flow line. The thickness distribution $nt/2\pi R$ is taken similar to that at the tip, with a possible variation in the maximum thickness along the radius.

The flow variations from hub-to-shroud are obtained with the flow considered two-dimensional (i.e., axisymmetric) with the streamlines

projected on the radial-axial (i.e., meridional) plane. The approach to the problem is to determine for successive streamlines the distribution of pressure and velocity from the tip toward the inner shroud along lines of constant z. Successive streamlines are computed until the desired entrance mass flow is obtained. The resultant inner streamline shape then represents the required hub contour.



Radial equilibrium. - The flow variations along R at any point are obtained by consideration of the radial component of Euler's equation (eq. (2a), ref. 9, e.g.). This equation may be expressed in terms of the relative velocity components for time-steady relative flow as

$$\frac{1}{\gamma\rho}\frac{\partial p}{\partial R} = \frac{(M_t R + Q_\theta)^2}{R} - Q_z\frac{\partial Q_r}{\partial z} - Q_r\frac{\partial Q_r}{\partial R} - \frac{Q_\theta}{R}\frac{\partial Q_r}{\partial \theta} \tag{7}$$

Since

$$\frac{dQ_r}{dS} = \frac{1}{Q}\left(Q_z\frac{\partial Q_r}{\partial z} + Q_r\frac{\partial Q_r}{\partial R} + \frac{Q_\theta}{R}\frac{\partial Q_r}{\partial \theta}\right)$$

equation (7) becomes

$$\frac{1}{\gamma\rho}\frac{\partial p}{\partial R} = \frac{(M_t R + Q_\theta)^2}{R} - Q\frac{dQ_r}{dS} \tag{8}$$

along the prescribed streamline. The value of $Q_r$ at each z-station along the streamline may be computed from the known mean velocity and flow directions $\beta$ and $\varphi$, since

$$Q_r = \frac{Q\cos\beta'\tan\varphi}{\sqrt{1 + \cos^2\beta'\tan^2\varphi}} \tag{9}$$

The term $dQ_r/dS$ is approximated by the use of finite differences. Then

$$\frac{dQ_r}{dS} \approx \frac{\Delta Q_r}{\Delta S}$$

where

$$\Delta S = \frac{\Delta z\sqrt{1 + \cos^2\beta'\tan^2\varphi}}{\cos\beta'}$$

From the previously specified conditions for the tip streamline, the radial gradient in pressure may be determined.

Continuity in meridional plane. - Progressing from the tip streamline toward the hub is accomplished by considering the successive streamlines a short radial distance $\Delta R$ apart. The continuity equation for this stream filament may be written as

$$\Delta W = \frac{2\pi}{n} \int_{R-\Delta R}^{R} \frac{\rho Q \cos \beta' R}{\sqrt{1 + \cos^2\beta' \tan^2\varphi}} \left(1 - \frac{nt}{2\pi R}\right) dR \qquad (10)$$



The values of $\rho$, $Q$, and $\beta'$ are known at the tip radius. Approximating a mean value between $R$ and $R-\Delta R$ by expressing the term

$$\frac{\rho Q \cos \beta' R}{\sqrt{1 + \cos^2\beta' \tan^2\varphi}} \left(1 - \frac{nt}{2\pi R}\right)$$

with a Taylor's expansion from the known conditions on the boundary and using the first two terms of the expansion in equation (10) give

$$\frac{n\Delta W}{2\pi} \approx \frac{\rho Q \cos \beta' R}{\sqrt{1 + \cos^2\beta' \tan^2\varphi}} \left(1 - \frac{nt}{2\pi R}\right) \left\{ \Delta R - \frac{\Delta R^2}{2} \left[ \frac{1}{\rho} \frac{\partial \rho}{\partial R} + \frac{1}{Q} \frac{\partial Q}{\partial R} - \right.\right.$$

$$\left.\left. \tan \beta' \frac{\partial \beta'}{\partial R} + \frac{1}{R} + \frac{\partial}{\partial R} \ln \left( \frac{1 - \frac{nt}{2\pi R}}{\sqrt{1 + \cos^2\beta' \tan^2\varphi}} \right) \right] \right\} \qquad (11)$$

The term $\tan \beta' \frac{\partial \beta'}{\partial R}$ is fixed by the condition that the mean flow path lies on a prescribed radial surface. The term $\frac{1}{\rho} \frac{\partial \rho}{\partial R}$ is determined from equation (8); $\frac{1}{Q} \frac{\partial Q}{\partial R}$ may then be obtained by differentiating equation (3) along $R$. The incremental weight flow $\Delta W$ entering a stream tube may be determined from equation (11) by substituting conditions determined at the rotor entrance and selecting an incremental $\Delta R_1$. Equation (11) then may be solved as a quadratic for $\Delta R$ for all other stations through the rotor. By subtracting $\Delta R$ from the tip radius, the projection of the next lower streamline in the meridional plane is determined. Flow conditions along this streamline are obtained from conditions at the tip by extrapolating across $\Delta R$ with the gradient obtained in equation (8). Solutions of equations (8) and (11) are then carried

out on this next lower streamline, progressing down into the flow field by successive increments in $\Delta R$ until the desired rotor weight flow is included between the tip and hub streamline.

In general, the accuracy of a solution carried out as described above might be expected to be improved by use of small incremental distances or by use of successive approximations to obtain a more accurate mean value for equation (11). For supersonic flow, this system must in all cases be considered at best an approximation, since discontinuities of even the first derivatives of the flow conditions (i.e., $\rho$, $Q$, and $\beta'$) may occur across a Mach line. In addition, by the assumption of a continuous variation in the flow conditions, disturbances in the flow are not confined to the Mach cone but propagate generally throughout the flow. However, if the prescribed tip velocities vary gradually and continuously, then the flow for some distance down from the tip has been assumed to be shock-free with continuous derivatives. A further objection arises in that, from experience, any errors occurring in the calculation will be cumulative. For these reasons, the method is not recommended for rotors of low hub-inlet radius ratios (i.e., below about 0.6).



Rotor-entrance annulus. - In order to establish the desired flow conditions at the entrance to the compressor rotor, the solution of the upstream annulus can be made at the same time as that for the rotor. The equations governing the flow are of the same form as those used inside the rotor, although the freedom in selecting conditions is necessarily much restricted. To conform with the rotor design, the outer-wall contour and either a prescription of the velocities on the outer wall or a uniform continuation of the height $\Delta R$ of the tip stream tube may be made. The only remaining freedom of selection is in the tangential-velocity (or $rV_\theta$) distribution along the radius at a single axial position.

The flow equations take the following form for use in the entrance section:

Continuity:

$$\frac{n\Delta W}{2\pi} \approx \frac{\rho V \cos\beta\, R}{\sqrt{1 + \cos^2\beta \tan^2\varphi}} \left[\Delta R - \frac{\Delta R^2}{2}\left(\frac{1}{\rho}\frac{\partial \rho}{\partial R} + \frac{1}{V}\frac{\partial V}{\partial R} - \tan\beta \frac{\partial \beta}{\partial R} + \frac{1}{R} + \frac{\partial}{\partial R} \ln \frac{1}{\sqrt{1 + \cos^2\beta \tan^2\varphi}}\right)\right] \tag{12}$$

Energy:

$$\rho = \left(1 - \frac{\gamma - 1}{2} V^2\right)^{\frac{1}{\gamma - 1}} \tag{13}$$

Radial component of Euler's equation:

$$\frac{1}{\gamma\rho}\frac{\partial p}{\partial R} = \frac{V_\theta^2}{R} - \frac{V\,dV_r}{dS} \tag{14}$$

The tangential velocity along any streamline will be fixed by the conservation of moment of momentum and the prescribed $rV_\theta$ distribution. The solution of the upstream annulus follows in a manner identical to that for the rotor. The gradients of the flow conditions are obtained at the tip from equation (14), and the next lower streamline is determined on the basis of continuity (eq. (12)). The flow conditions are then found on the next lower streamline and the solution repeated for a second incremental stream tube, the process being continued until the required mass flow is contained in the annulus.



Matching flow conditions at rotor leading edge. - At the entrance to the rotor, the relative streamline direction should be continuous in passing from upstream of the rotor into the rotor passage. In addition, there should be no discontinuity in the streamline direction in the meridional plane. At the tip the position of the leading edge is known from the prescribed conditions. At all other radii, the position of leading edge must be determined so that the relative stream surface is continuous in entering the blade passage. The following method is suggested:

(1) After solving for the flow in the upstream entrance section, compute the relative flow direction in the vicinity of the leading edge from

$$\tan \beta' = \frac{V_\theta - M_t R}{V_z}$$

(2) From the mean flow surface determined for the rotor, make a plot of $\tan \beta'$ against $z$ and find the z-position at which the mean flow direction matches the inflow angle. This position is then used as the leading edge of the rotor blade.

(3) The blade-thickness distribution in the region near the leading edge is then adjusted so that the streamline in the meridional plane passes smoothly from the entrance section into the rotor.

## Application of Design Method

Rotor tip conditions. - The design method described in the previous section was used to design the rotor for this investigation. The following specifications were used to obtain the design conditions:

(1) Rotor tip speed, 1600 ft/sec in air

(2) Axial discharge relative to rotor at all radii

(3) Constant rotor tip radius

(4) Tip-section entrance Mach number, $M_{z,1}$, 0.70

(5) Zero prewhirl

(6) Inlet hub-tip radius ratio, 0.75





Approximate vector diagrams at the entrance and exit were selected for the mean radius for the condition of equal entrance and exit relative velocities. The high absolute tangential velocity at the rotor exit resulted in a large gradient in static pressure. In order to satisfy radial equilibrium and to establish the desired mean exit velocity, an increase was required in the tip static pressure at the rotor exit over that prescribed at the entrance. This change in static pressure and the corresponding velocity change along the tip streamline were distributed linearly in the z-direction (fig. 2). The absolute tangential velocity at the tip was specified as shown in figure 3(c); it rose rapidly from zero and leveled off at the discharge value near the rotor discharge (the resultant distribution of mean surface flow angle is shown in figure 3(b). In order to determine the stream-tube height $h$ at the exit, an allowance of 10 percent of the flow passage was made for the blade wake and boundary layer. The distribution of $h$ was then specified as shown in figure 3(d). The blade thickness term, incorporating the boundary-layer and wake allowance that resulted from the prescribed $Q$, $V_\theta$, and $h$ ratios, is shown in figure 3(a). The blade-surface velocity ratios obtained for 29 rotor blades are shown in figure 2, along with the specified mean flow velocity ratio.

Tip-to-hub solution. - The solution inside the impeller passage was carried out as described, equation (11) being used to obtain $\Delta R$ from the tip streamline to the streamline adjacent to the tip. The velocity distribution on this streamline was obtained from equations (8) and (3) and the velocities at the tip streamline. The slope of the streamline $\varphi$ was obtained with finite differences. These slopes were plotted against $z$, and interpolation was made graphically; $Q_r$ was then found as a function of $z$, from equation (9). The process was continued for successively lower streamlines to the desired inlet hub-tip radius ratio.

The meridional streamline configuration is shown in figure 4. The mean velocity distribution at the hub and the approximate blade loading obtained from equations (5) and (6) are shown in figure 5.

Blade shape. - The computational method used only the mean flow angle and a thickness distribution that included blade thickness plus a displacement thickness allowance. The blade shape must then be selected to give the desired mean flow angle.

For high-solidity blading, the blade mean line can be expected to correspond very closely to the flow mean line, except in the entrance and exit portions. At the entrance of supersonic compressors, two-dimensional considerations (ref. 10) indicate that for straight blades, the flow should enter parallel to the suction surface of the blade. Curvature of the blade suction surface will tend to decrease the inlet flow angle from that for a straight blade. The effect of the contracting passage height was not certain, although it was expected to reduce the effect of the curvature behind the leading edge. As a compromise, the blade leading-edge mean angle was adjusted so that the suction surface at the leading edge was parallel to the desired mean flow angle.

The boundary-layer allowance was made entirely on the suction surface, with a linear build up of the boundary-layer displacement thickness assumed in the z-direction from rotor entrance to discharge. The resulting blade shape is shown in figure 6.

At the design operational conditions for this rotor, the equivalent air weight flow was 18.4 pounds per second per square foot of frontal area. For isentropic flow through the rotor, the discharge Mach number at the mean radius was 2.03, and the pressure ratio was 6.9.

## APPARATUS AND INSTRUMENTATION

Variable-component test rig. - This impulse-type supersonic-compressor rotor was installed in the variable-component test rig as described in reference 1. The data presented were obtained by using Freon-12 (dichlorodifluoromethane) as the testing medium. A schematic diagram of the installation is shown in figure 7, and a photograph of the compressor rotor installed in the variable-component test rig is shown in figure 8. The passage height behind the rotor is 0.855 inch and extends back about $1\frac{1}{4}$ inches. To avoid choking of the rotor flow in the downstream annulus, the passage height was increased by tapering the inner wall down to a diameter of $10\frac{3}{8}$ inches, while the outer diameter remained constant at 16 inches.

Instrumentation. - The over-all rating of the compressor rotor, the weight flow, and the inlet stagnation conditions were all obtained as described in reference 1. A cone-type instrument was used to obtain

flow angles and total pressures; and a double-stagnation-type probe was used to obtain total temperatures. These two instruments (fig. 9) were installed at instrument station 2 about 0.75 inch behind the rotor. In addition to these instruments, wall static taps along the flow passage and at the survey station were utilized to obtain static pressures.

Because it was necessary to maintain a Freon-12 purity of at least 0.97 by volume, a purity analyzer that measured change in electric conductivity of the mixture was used to determine the content of the test gas.

## PROCEDURE



The compressor rotor was operated over a range of speeds from 48.7 to 97.5 percent of design in Freon-12. The rotational speed in Freon-12 was computed to obtain the design relative entrance Mach number at the compressor tip. Constant inlet temperatures of 100° F (±1.0°) and inlet pressure of 30.0 inches mercury absolute (±0.1 in. Hg) were maintained by the automatic controls of the previously mentioned test apparatus. Compressor-rotor back pressures were obtained by the sliding throttle shown in figure 7.

The compressor rotor was rated on the conditions in the depression tank and the survey data obtained directly behind the rotor at station 2. Instrument station numbers are indicated in figure 7. The computational methods used are described in reference 1.

The compressor rotor was originally installed with a straight discharge annulus; however, a check of the static-pressure profile over the rotor indicated that the rotor could not be operated at the design impulse condition. Expanding the discharge passage as described previously permitted design impulse operation at the open-throttle condition. All the data included in this report were obtained with the expanding discharge passage.

The consistency of the data may be judged by a comparison of the weight flow or of the work input obtained at 97.5-percent design speed, open-throttle or impulse condition, as follows:

| Method | Work input, Btu/lb |
|---|---|
| Measured temperature rise | 19.21 |
| Change in angular momentum | 19.61 |
| Electrical power to motor | 20.02 |
| **Measurement** | **Weight flow, lb/sec Freon-12** |
| Calibrated nozzle | 48.55 |
| Survey at instrument station 2 | 49.30 |

The above comparison of measurements is typical of all open-throttle or impulse conditions. However, the high-back-pressure points do not obtain this same consistency.

## DISCUSSION OF PERFORMANCE

### Over-All Performance

Performance of the rotor as a separate component was obtained in Freon-12, and the results are presented in figure 10 for the seven rotational speeds of this investigation. At 97.5-percent design speed and impulse operation a peak total-pressure ratio of 5.7 was obtained with an adiabatic efficiency of about 0.89; the absolute mean-radius discharge Mach number was about 1.93. The equivalent weight flow of 48.55 pounds per second of Freon-12 corresponds to about 26.2 pounds per second of air. The rotor operates at essentially a constant weight flow for the higher rotational speeds (92.5 and 97.5 percent of design) and over a small range of total-pressure ratios and adiabatic efficiencies. The rotor characteristics at reduced rotational speeds (87.6 to 48.7 percent of design) show an increasing range of equivalent weight flows at almost constant total-pressure ratios. Peak adiabatic efficiency for each speed is obtained at peak total pressure and maximum equivalent weight flow for all except the 48.7- and 58.4-percent design speeds. A maximum adiabatic efficiency of about 0.90 is obtained for impulse operation at 92.5-percent design speed with a total-pressure ratio of about 5.1.

2778

### Rotor-Entrance Conditions

The design weight flow for this rotor is very nearly obtained at 97.5-percent design speed (computed for design speed of Freon-12, 49.6 lb/sec; measured for 97.5-percent design speed, 48.5 lb/sec). The computation of the design weight flow made no allowance for boundary layer or flow blockage.

To obtain the relative entrance flow conditions at the rotor tip and hub, the absolute velocity at the rotor entrance was computed with static-pressure measurements 1/2 inch ahead of the rotor blade with corrections for the area change from the measuring station to the leading edge. The relative Mach number and flow angle obtained in this manner are shown in figure 11 for the open throttle at 97.5-percent design speed, along with the design relative Mach number and the blade suction- and pressure-surface angles at the leading edge. The relative entrance flow angle computed from wall static pressures is about $2\frac{1}{2}^{\circ}$ less (negative angle of attack) than the design inlet flow angle at the

tip and about 2° less at the hub section. This deviation from the angle of the suction surface is in the direction that might be expected for curved blades, as discussed in reference 10, and indicates an excessive allowance for the effect of the contracting passage height.

## Static-Pressure Profiles



The static-pressure profile over the outside rotor housing measured at open throttle and 97.5-percent design speed is compared with the design static pressure along the rotor tip section in figure 12. The static-pressure rise is all obtained over the first 20 percent of the rotor rather than the gradual pressure build-up as designed. However, the over-all static-pressure rise is close to the design value. Since the tip section is operating at a negative incidence, there is a decrease in flow area as the fluid enters the rotor passage. This area decrease can account for about one-half that required to obtain the measured increase in static pressure at the rotor entrance (fig. 12). Other factors that could influence the static pressure near the leading edge are (1) the oblique shock arising from the finite leading-edge wedge angle, (2) disturbances arising from the hub contour, and (3) flow separation from the blade or casing followed by a reattachment.

## Discharge Conditions

In figure 13(a) the total-pressure ratio, adiabatic efficiency, and comparative work input $\Delta H/U_t^2$ for this compressor rotor at the impulse or open-throttle condition are shown for the range of rotational speeds of this investigation. The total-pressure ratio continues to increase at an increasing rate as the speed is increased. The adiabatic efficiency increases slightly with speed and reaches a peak value of 0.90 at 92.5- and 97.5-percent design speed. For the open-throttle condition shown, the work input is almost constant over the speed range and almost equal to the design value.

The mean-radius discharge conditions measured for this rotor at the impulse or open-throttle conditions over the speed range are shown in figure 13(b). The design values are the theoretical isentropic conditions of the free stream. The pitch-section axial discharge Mach number increases at a continuously increasing rate until it is about 1.35 at 97.5-percent design speed. This value is to be compared with a design value for the free stream of about 1.49. The observed conditions represent an average of the free stream and wake, and will, of necessity, be lower than the isentropic free-stream value. Also, for the same reason, the absolute discharge Mach number is slightly below the design, and the absolute discharge flow angle is about 4.0° higher than the design flow angle.

Discharge Surveys

Measured discharge conditions over the annulus are compared with the design values (impulse operation and 97.5-percent design speed) in figure 14(a). The comparative work input $\Delta H/U^2$ based on the temperature measurements is somewhat higher than the design value at the compressor hub and tip sections. Over the rest of the radius the comparative work input is slightly below the design value. This large work input measured at the hub allows the pressure ratio at the hub to be equal to the design value at less than 100-percent efficiency and 97.5-percent design speed. The fact that the pressure ratio decreases at the increasing radii, rather than increasing according to the design curve, is a result of increasing losses, as indicated by the decrease in adiabatic efficiency toward the compressor tip. The mass-flow distribution over the passage, indicated by the $\rho V_{z,2}$ curve, shows that appreciable boundary layers exist at both the inner and outer walls.



The relative discharge Mach number and flow angle at 97.5-percent design speed are compared with the design values along the compressor-discharge radius in figure 14(b). The relative discharge Mach number is below the design value. Since the design value was that computed for ideal free-stream conditions, losses on the rotor would reduce the observed relative Mach number. Thus the decrease in relative discharge Mach number toward the tip reflects the increased losses indicated by the adiabatic-efficiency distribution. The relative discharge flow angle is about $2^\circ$ less than axial at the tip section. The flow angle increases toward the hub, where the relative flow direction is about $8^\circ$ past the axial. This deviation in flow angle relative to the rotor blade may be due to secondary or radial flows or relative fluid rotation such as that considered in reference 11.

The absolute discharge Mach number and flow angle used in calculating the relative conditions are included in figure 14(b). The Mach number is below design at the tip and slightly above design at the hub section. The measured flow angle is from $3^\circ$ to $4^\circ$ higher than the design angle, except at the hub, where it is considerably higher than design. The design computations were carried out for air; the comparison of design at test discharge conditions was made by correcting the air design to Freon Mach numbers according to the area ratios along each stream filament. The observed performance for this rotor indicates good efficiencies for the rotor as a separate component. The performance of a complete stage, however, will depend to a large extent upon the losses that occur in the stators when an attempt is made to recover the energy contained in the very high absolute discharge Mach number.

## SUMMARY OF RESULTS

An approximate, quasi-three-dimensional design procedure has been applied to high-solidity impulse-type supersonic compressors. The principle of zero absolute circulation for flows with no losses was used to determine blade-surface velocities. The stream-filament approach with the assumption of axisymmetric flow was used to obtain the streamline configuration in the hub-to-shroud plane.

The method was applied to a compressor rotor having a tip speed of 1600 feet per second in air, an inlet hub-tip radius ratio of 0.75, and an axial discharge relative to the rotor. The design pressure ratio at the mean discharge radius for isentropic flow was 6.9 with an absolute discharge Mach number of 2.03. A comparison of the design and experimental data for this rotor produced the following results:

1. For operation at 97.5-percent design speed and open-throttle condition, the rotor obtained a total-pressure ratio of 5.7 at an adiabatic efficiency of about 0.89. The absolute mean-radius discharge Mach number was 1.93. At other than design speed, the level of adiabatic efficiency remains high.

2. The observed relative rotor-entrance flow angle was about $2^{\circ}$ less than the design flow angle.

3. The over-all static-pressure rise over the rotor was close to the design value; however, this static-pressure rise was obtained within about 20 percent of the compressor rotor entrance, rather than being distributed linearly.

4. The observed mean-section discharge conditions were reasonably close to the design values.

5. The observed losses were appreciably larger at the tip than at the hub section for this rotor, and as a result there were large discrepancies between measured and isentropically predicted values of Mach number, flow angle, and pressure ratio at the rotor tip section.

Although the rotor indicated good performance as a separate component, the performance of the complete stage will depend to a considerable extent on the mixing and diffusion losses encountered in the stators when diffusing from the discharge Mach number of about 1.9 to acceptable discharge velocities.

Lewis Flight Propulsion Laboratory
National Advisory Committee for Aeronautics
Cleveland, Ohio, June 26, 1953

## APPENDIX - SYMBOLS

The following symbols are used in this report:

| | |
|---|---|
| H | total enthalpy |
| h | ratio of annular height at any station to annular height at inlet, $\Delta R/\Delta R_1$ |
| M | Mach number |
| M' | relative Mach number |
| $M_tR$ | ratio of rotor speed at radius ratio R to upstream stagnation velocity of sound |
| n | number of blades |
| P | total (stagnation) pressure, lb/sq ft |
| p | ratio of stream (static) pressure to inlet stagnation pressure |
| Q | ratio of relative flow velocity to inlet stagnation velocity of sound |
| R | ratio of radius to rotor tip radius, $r/r_t$ |
| r | radius, ft |
| S | ratio of length along relative mean flow path to rotor tip radius |
| t | ratio of unavailable flow area taken up by blade thickness and boundary-layer displacement thickness to tip radius, measured in tangential direction |
| U | rotor speed, ft/sec |
| V | ratio of absolute flow velocity to upstream stagnation velocity of sound |
| $V_{\theta,1}$ | ratio of absolute tangential flow velocity at rotor entrance to upstream stagnation velocity of sound |
| W | weight flow, lb/sec |
| z | axial component |
| $\beta$ | absolute flow angle projected in z-$\theta$ (tangential) plane, measured positive in direction of rotation |

$\beta'$ projected relative flow angle in z-$\theta$ (tangential) plane, measured positive in direction of rotation

$\gamma$ ratio of specific heats

$\delta$ ratio of actual inlet stagnation pressure to sea-level pressure, $P_1/2116$

$\eta$ adiabatic efficiency

$\theta$ angular direction (coordinate system), positive in direction of rotation

$\sqrt{\theta}$ square root of ratio of actual inlet stagnation temperature to standard sea-level temperature, $T_1/518.6$

$\rho$ ratio of stream density to inlet stagnation density

$\varphi$ angle between flow direction and z-axis in R-z (meridional) plane

Subscripts:

m mean value

max maximum value

min minimum value

p pressure surface

r radial component

s suction surface

t tip

z axial component

$\theta$ tangential component

0 upstream measuring station, stagnation condition

1 station just ahead of rotor

2 station just behind rotor

REFERENCES

1. Ullman, Guy N., Hartmann, Melvin J., and Tysl, Edward R.: Experimental Investigation of a 16-Inch Impulse-Type Supersonic-Compressor Rotor. NACA RM E51G19, 1951.

2. Jacklitch, John J., Jr., and Hartmann, Melvin J.: Investigation of 16-Inch Impulse-Type Supersonic-Compressor Rotor with Turning Past Axial Direction. NACA RM E53D13, 1953.

3. Goldstein, Arthur W., and Schacht, Ralph L.: Performance of a Swept Leading Edge Rotor of the Supersonic Type with Mixed Flow. NACA RM E52K03, 1953.

4. Klapproth, John F., Ullman, Guy N., and Tysl, Edward R.: Performance of an Impulse-Type Supersonic Compressor with Stators. NACA RM E52B22, 1952.

5. Stanitz, John D.: Approximate Design Method for High-Solidity Blade Elements in Compressors and Turbines. NACA TN 2408, 1951.

6. Goldstein, Arthur W., and Mager, Artur: Attainable Circulation about Airfoils in Cascade. NACA Rep. 953, 1950. (Supersedes NACA TN 1941.)

7. Wright, Linwood C., and Klapproth, John F.: Performance of Supersonic Axial-Flow Compressors Based on One-Dimensional Analysis. NACA RM E8L10, 1949.

8. Stanitz, John D., and Prian, Vasily D.: A Rapid Approximate Method for Determining Velocity Distribution on Impeller Blades of Centrifugal Compressors. NACA TN 2421, 1951.

9. Wu, Chung-Hua: A General Theory of Three-Dimensional Flow in Subsonic and Supersonic Turbomachines of Axial-, Radial-, and Mixed-Flow Types. NACA TN 2604, 1952.

10. Kantrowitz, Arthur: The Supersonic Axial-Flow Compressor. NACA RRep. 974, 1950. (Supersedes NACA ACR L6D02.)

11. Stanitz, John D., and Ellis, Gaylord O.: Flow Surfaces in Rotating Axial-Flow Passages. NACA TN 2834, 1952.

2778

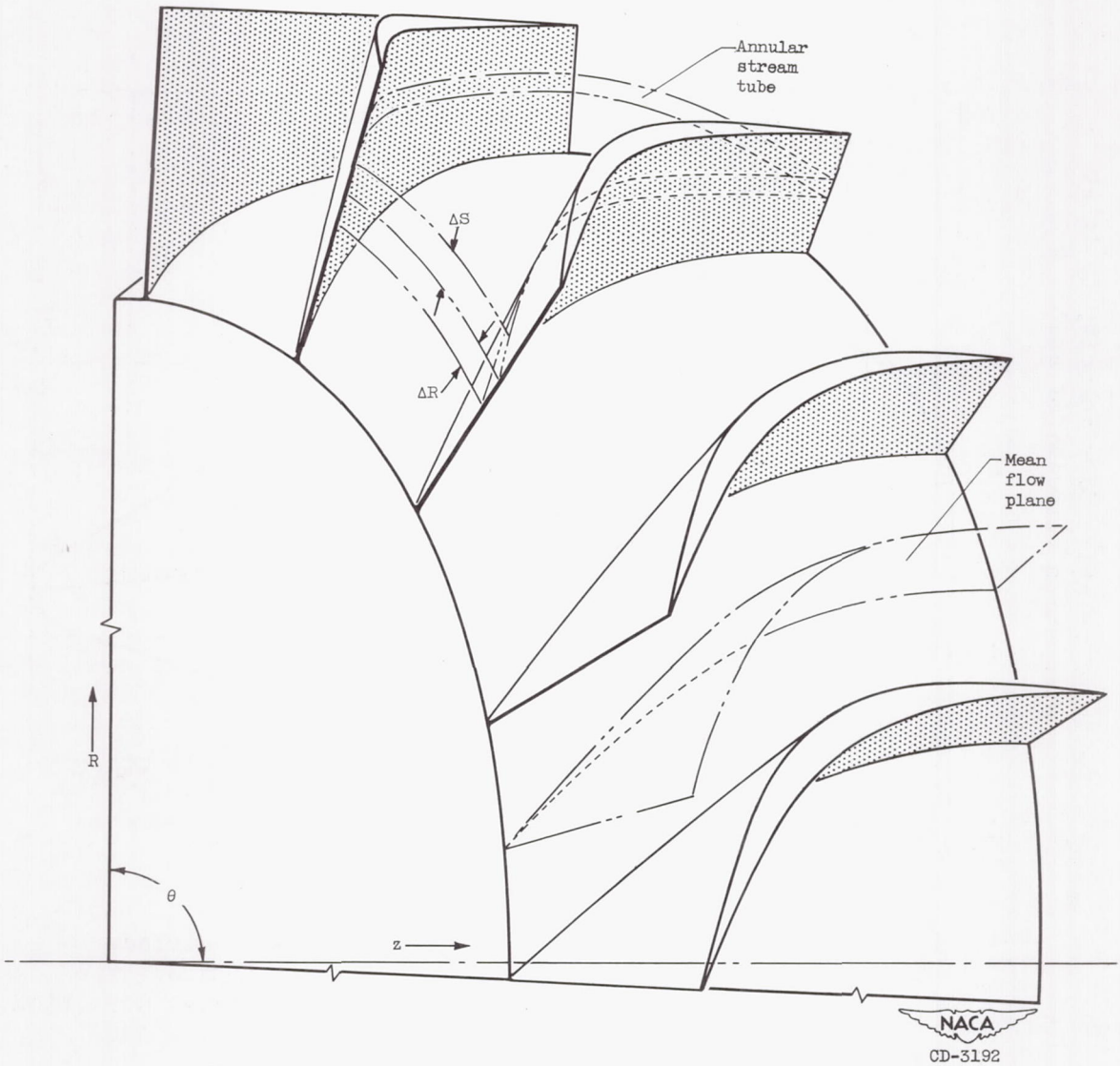


Figure 1. - Assumed flow surfaces through impluse-type supersonic compressor.

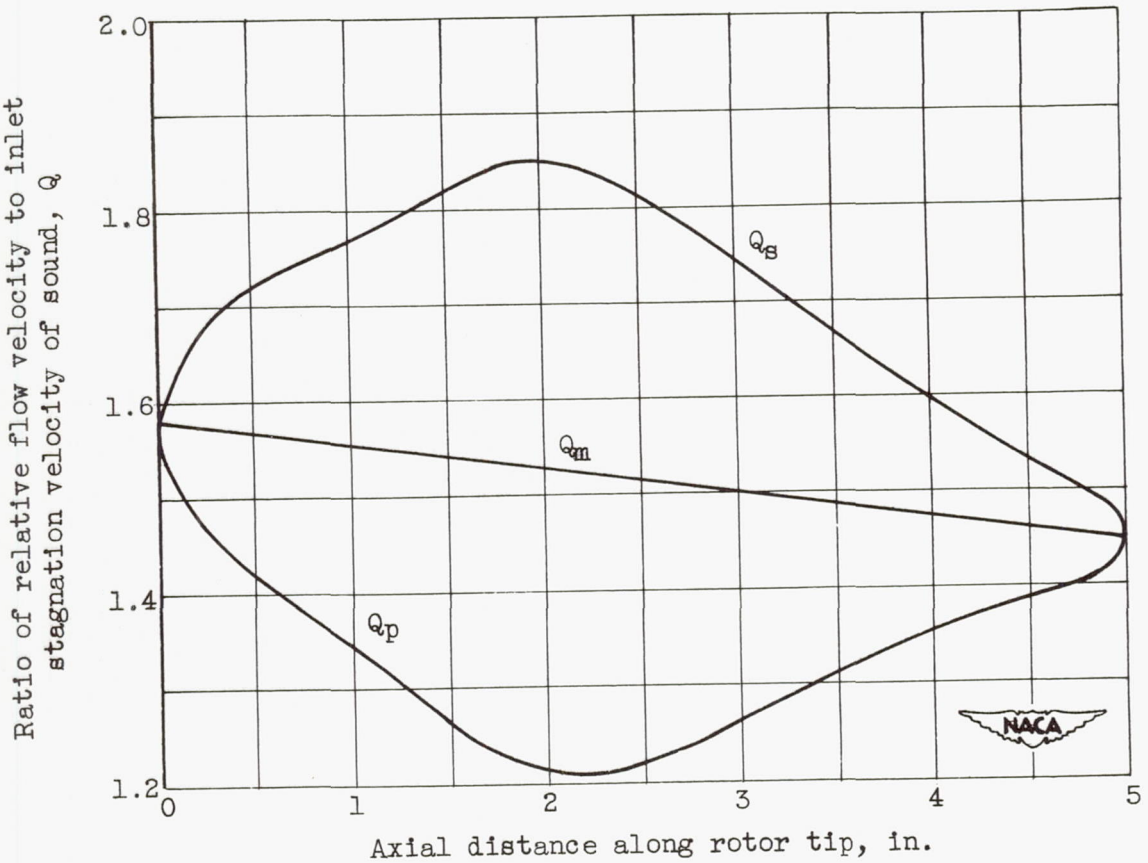


Figure 2. - Mean, suction-surface, and pressure-surface velocity ratios for tip section of 16-inch impulse-type supersonic-compressor rotor with turning to axial direction.

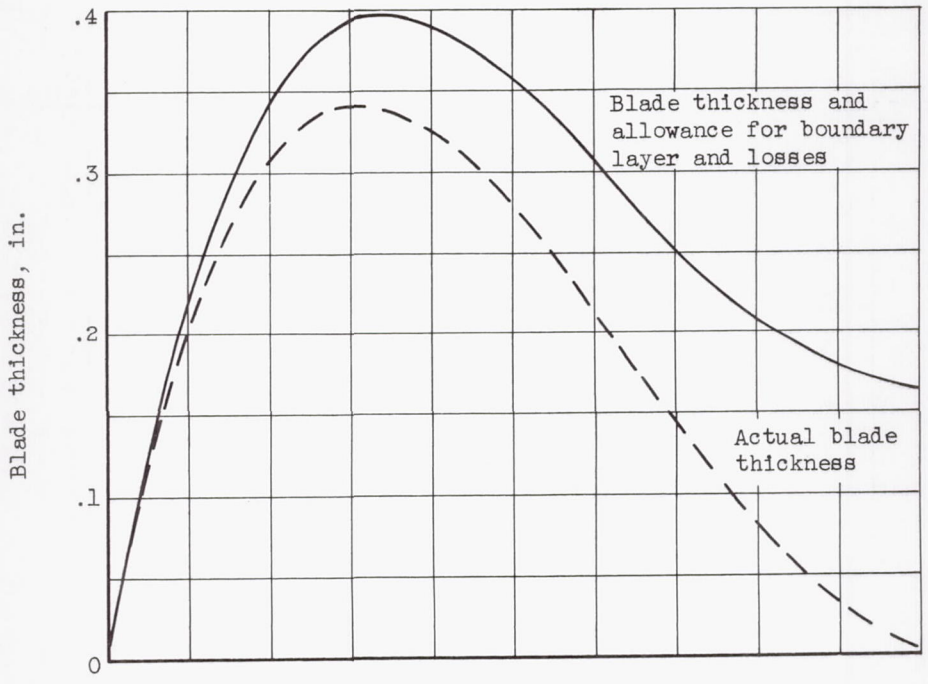


(a) Blade thickness.

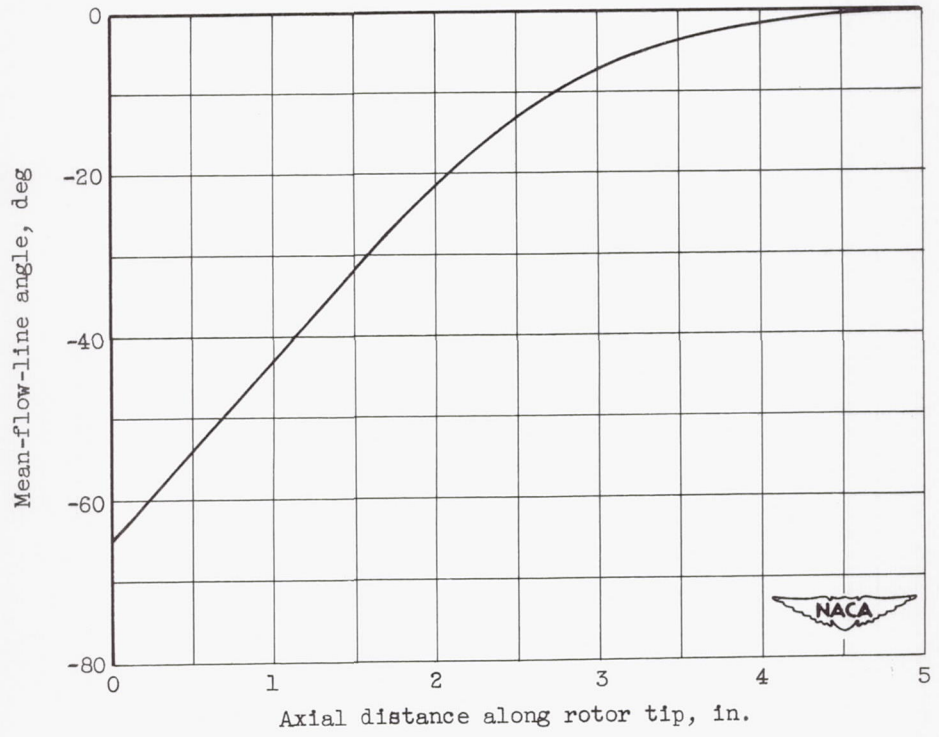


(b) Mean-flow-line angle.

Figure 3. - Tip conditions for 16-inch impulse-type supersonic-compressor rotor with turning to axial direction.

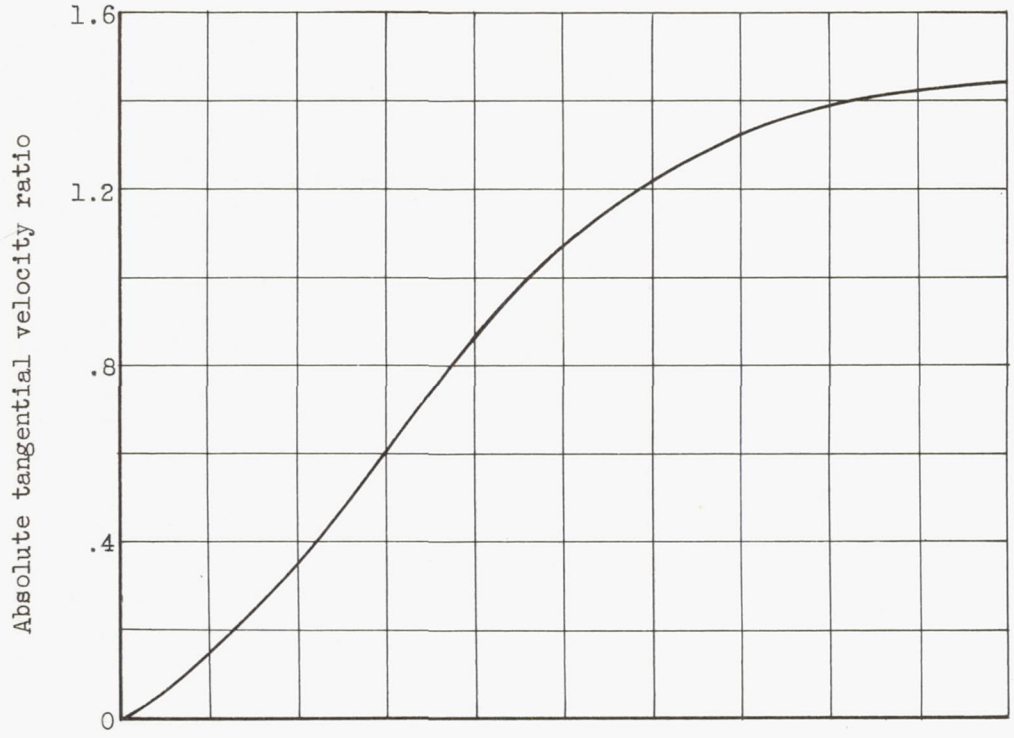


(c) Absolute tangential velocity ratio.

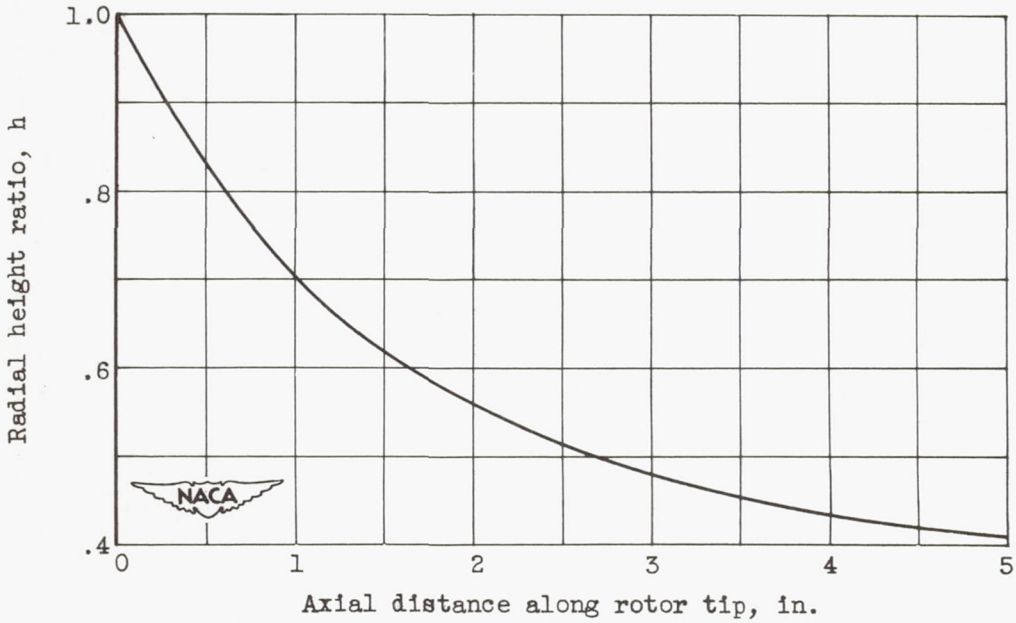


(d) Radial height ratio of tip section.

Figure 3. - Concluded. Tip conditions for 16-inch impulse-type supersonic-compressor rotor with turning to axial direction.

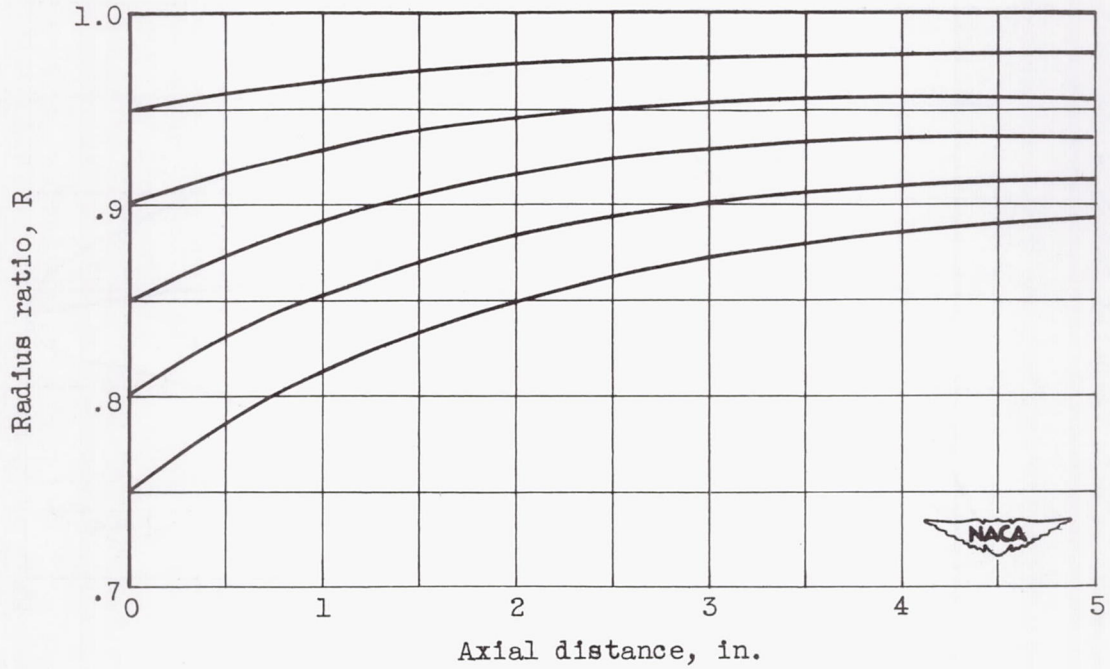


Figure 4. - Meridional streamline configuration for 16-inch impulse-type supersonic-compressor rotor with turning to axial direction.

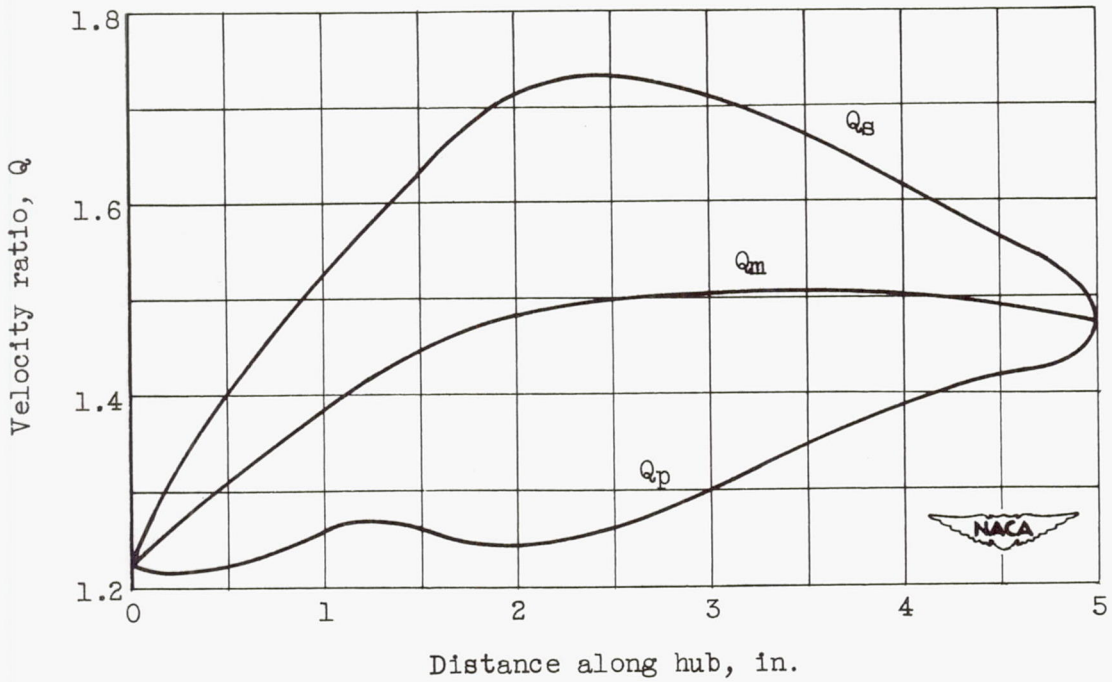


Figure 5. - Mean, suction-surface, and pressure-surface velocity ratios between blade surfaces at hub section of 16-inch impulse-type supersonic-compressor rotor with turning to axial direction.

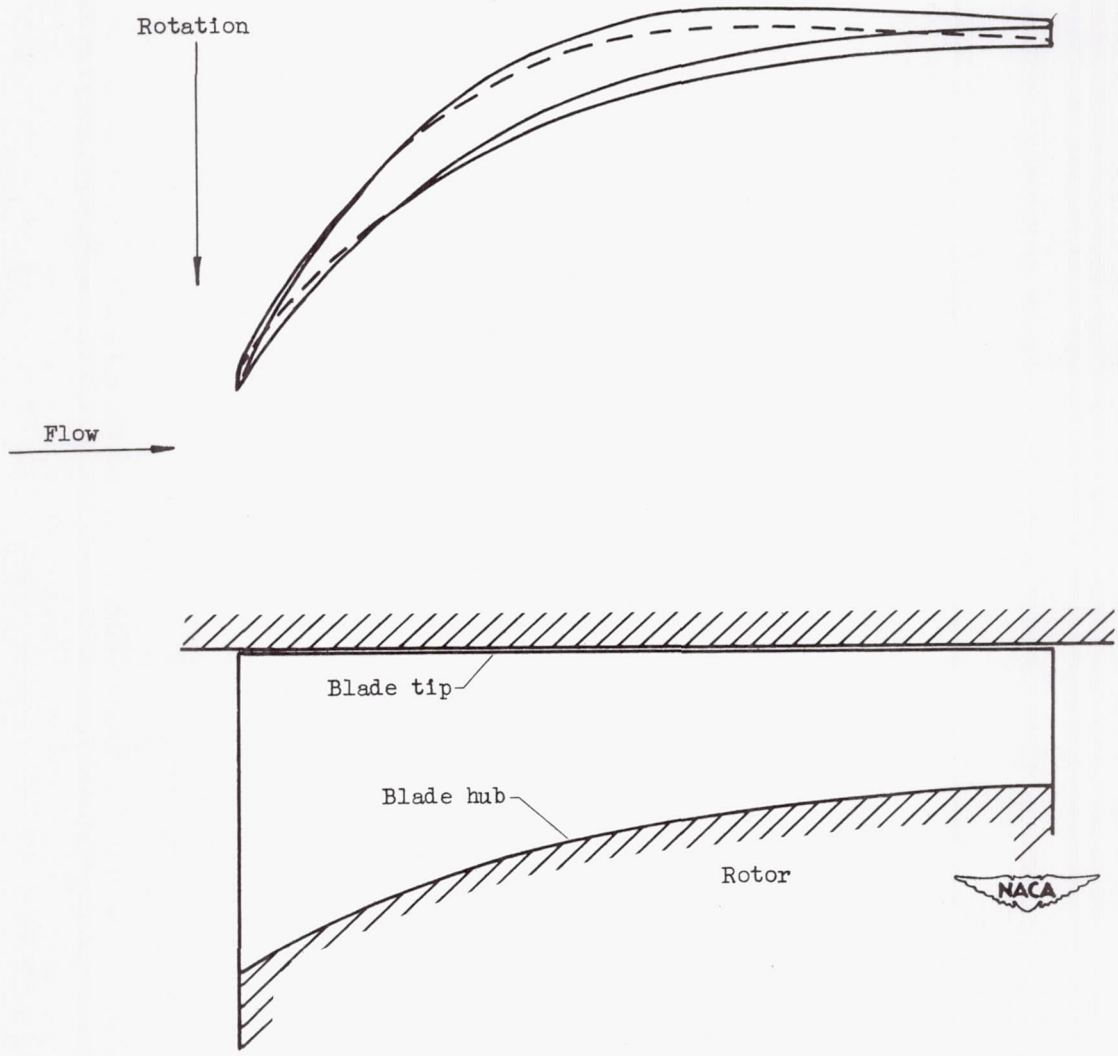


Figure 6. - Blade shape of 16-inch impulse-type supersonic-compressor rotor with turning to axial direction.

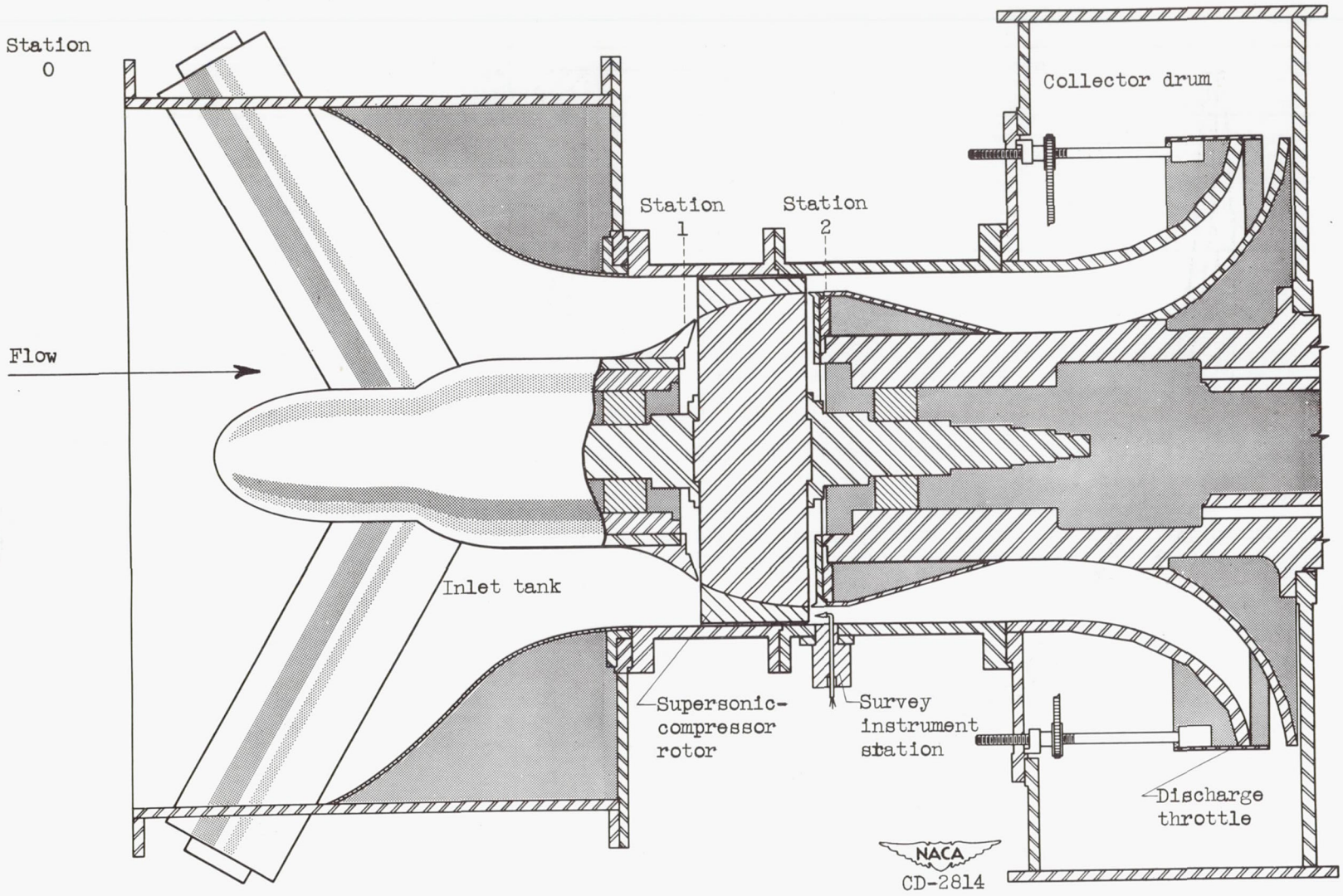


Figure 7. - Schematic diagram of 16-inch supersonic-compressor rotor installed in variable-component test rig.

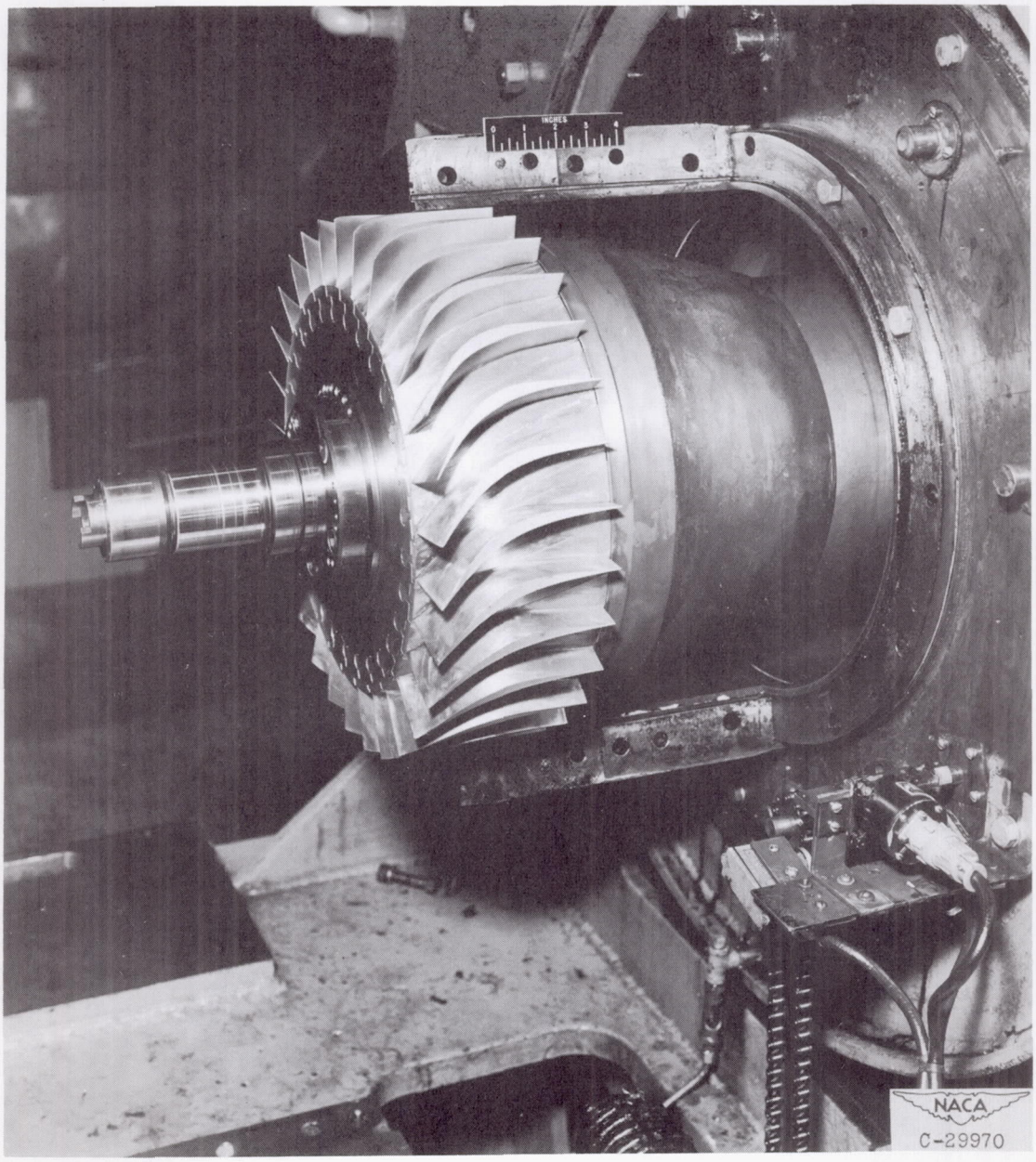


Figure 8. - 16-Inch impulse-type supersonic-compressor rotor installed in variable-component test rig.

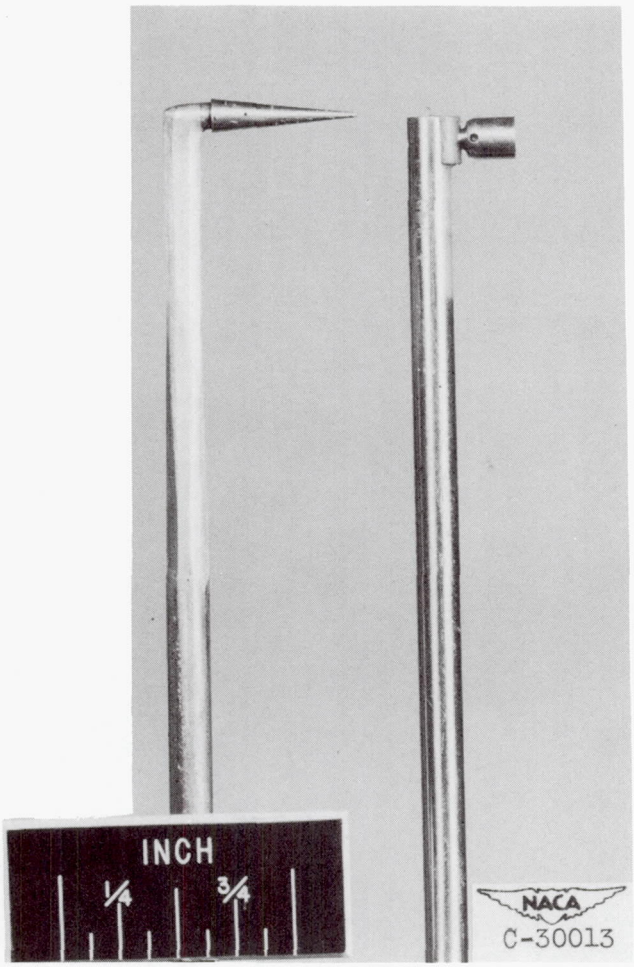


Figure 9. - Cone instrument and double-stagnation-type thermocouple used in investigation.

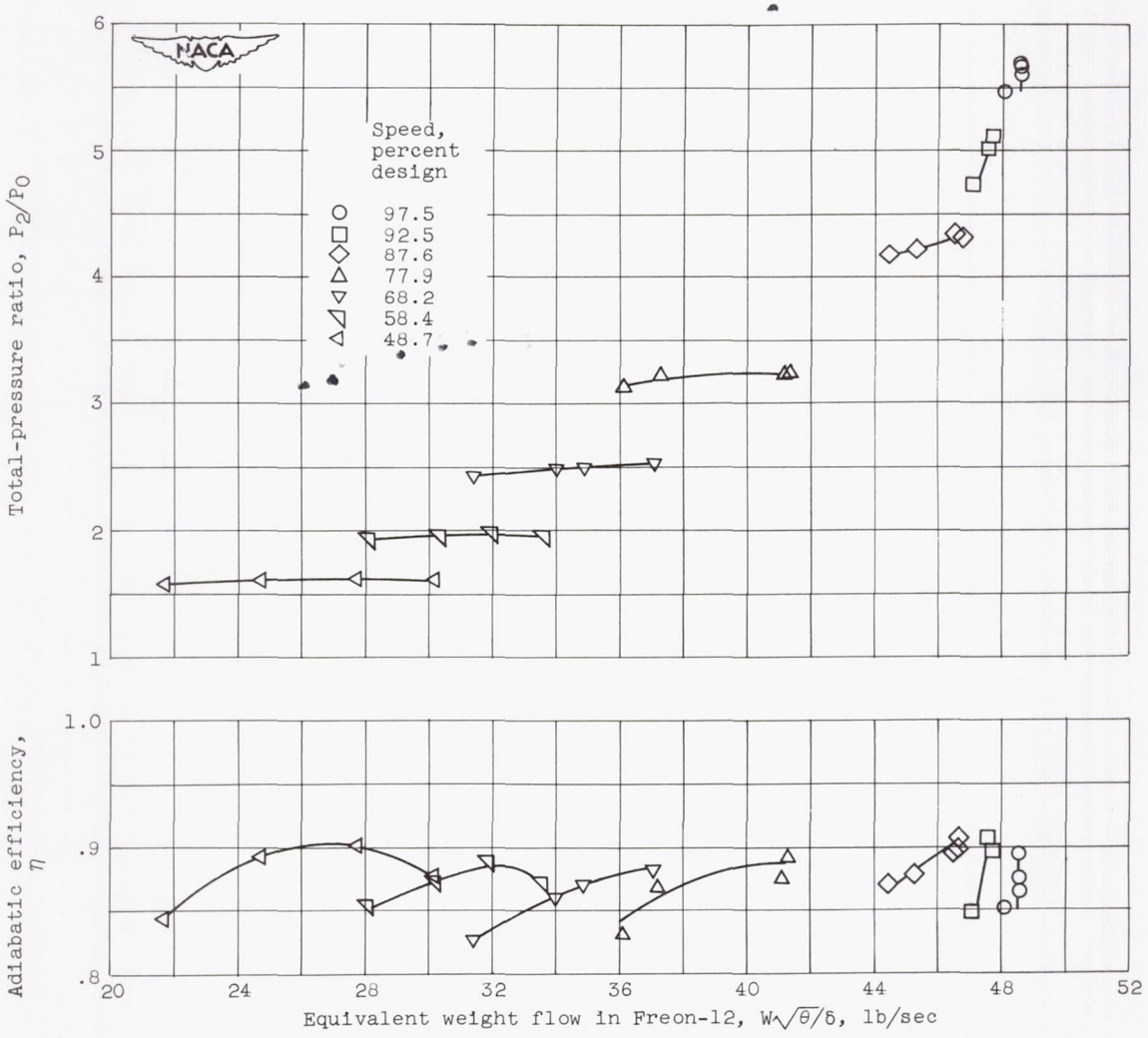


Figure 10. - Performance characteristics for 16-inch impulse-type supersonic-compressor rotor with turning to axial direction.

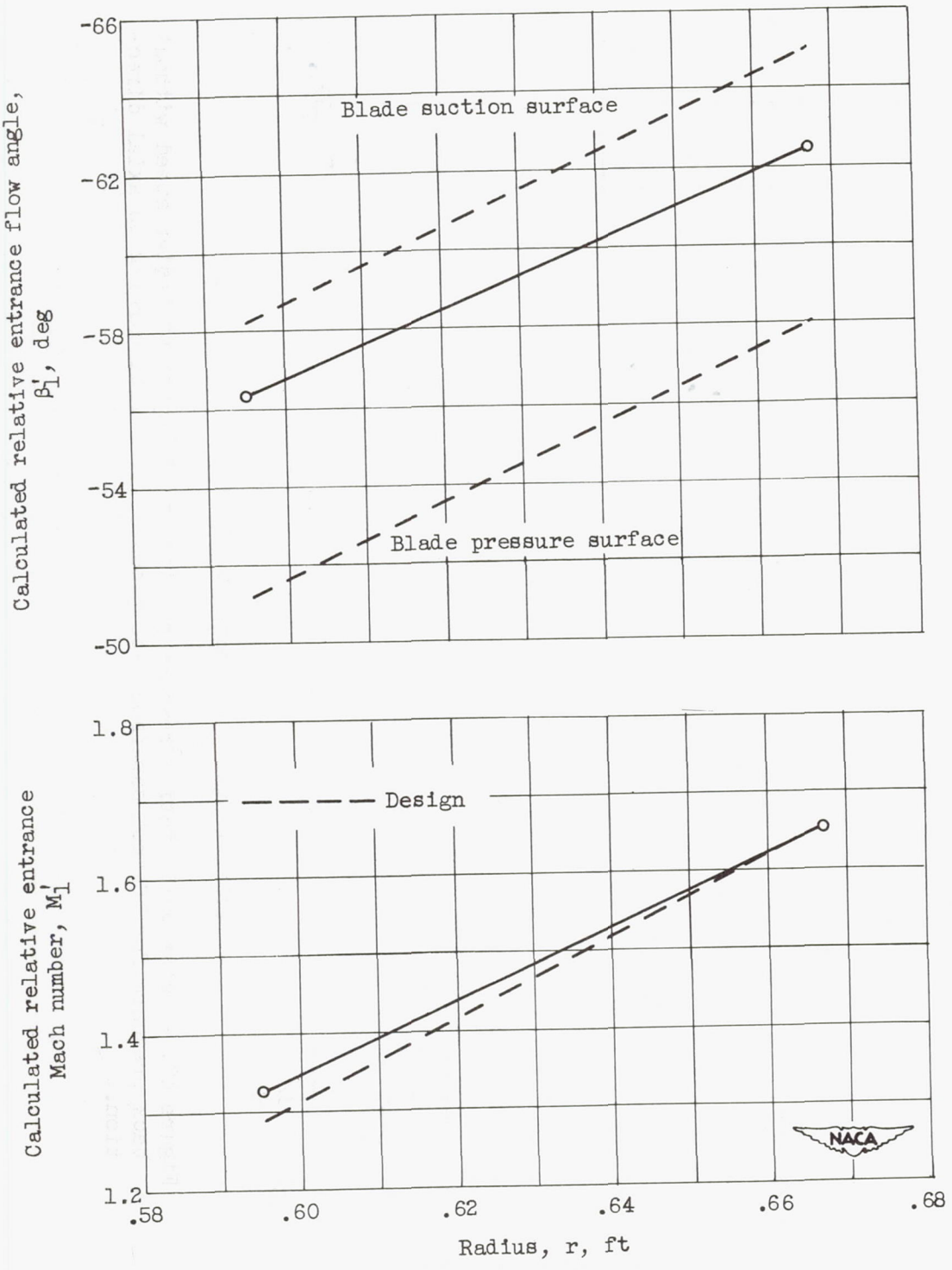


Figure 11. - Calculated relative entrance conditions at 97.5-percent design speed for 16-inch impulse-type supersonic-compressor rotor with turning to axial direction.

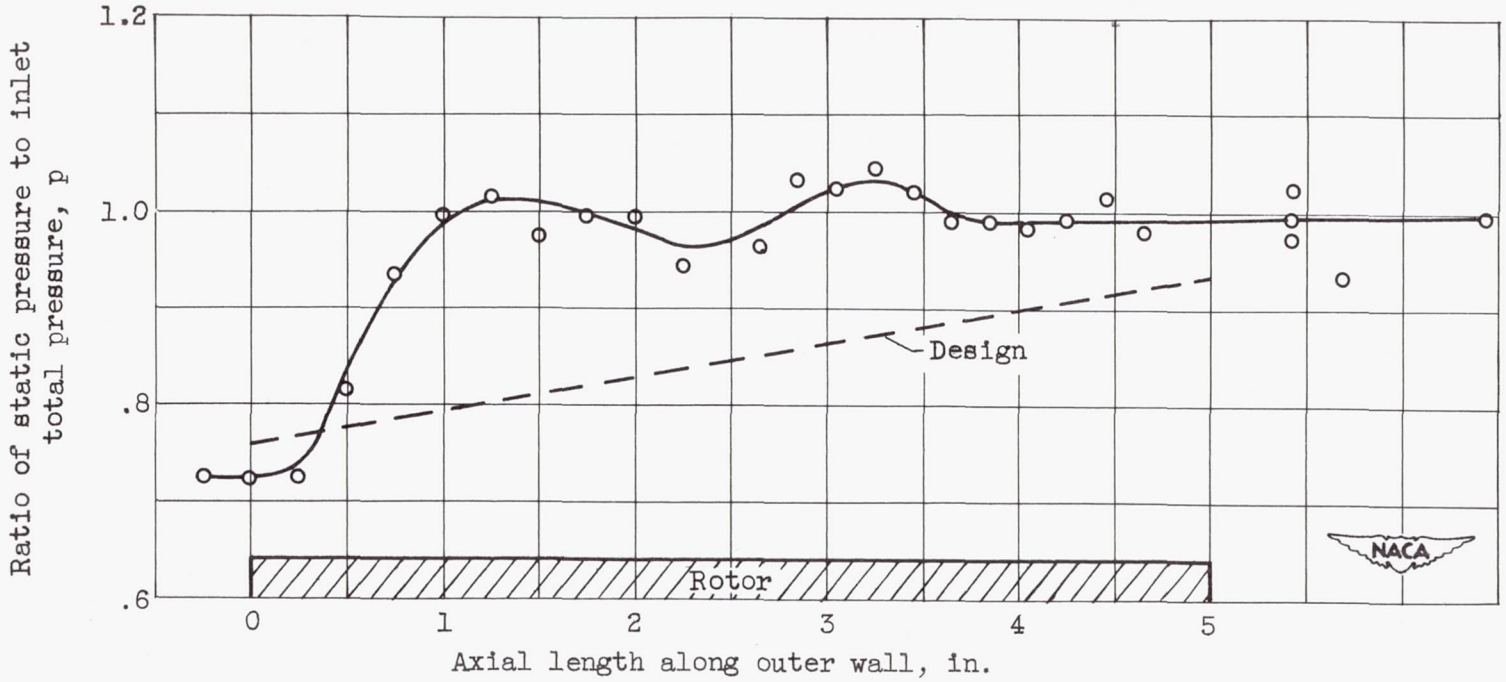


Figure 12. - Outer-wall static-pressure profile at 97.5-percent design speed without back pressure for 16-inch supersonic-compressor rotor with turning to axial direction.

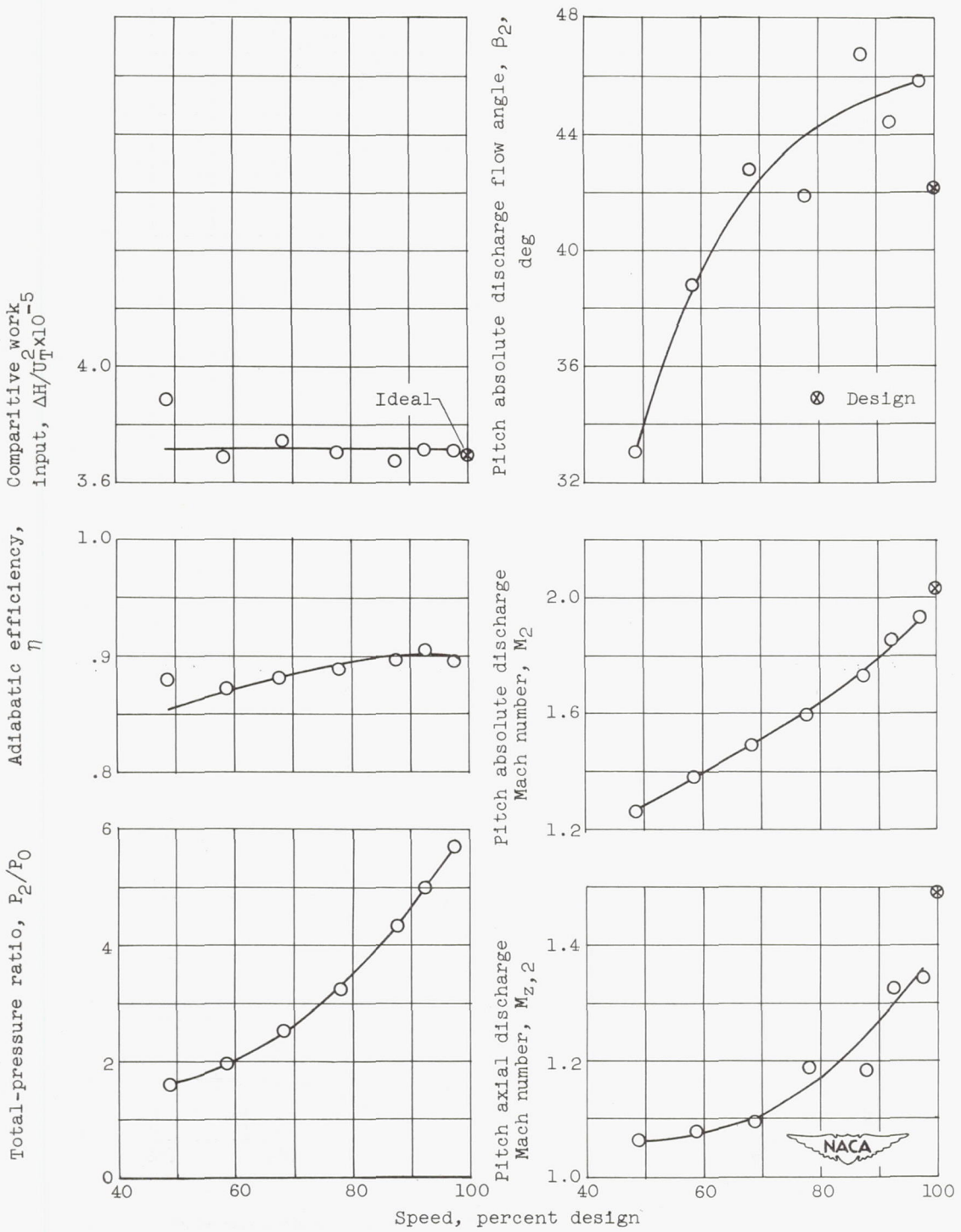


(a) Work input, efficiency, and total-pressure ratio.

(b) Pitch discharge flow angle and absolute and axial discharge Mach numbers.

Figure 13. - Impulse operation (open throttle) for 16-inch impulse-type supersonic-compressor rotor with turning to axial direction.

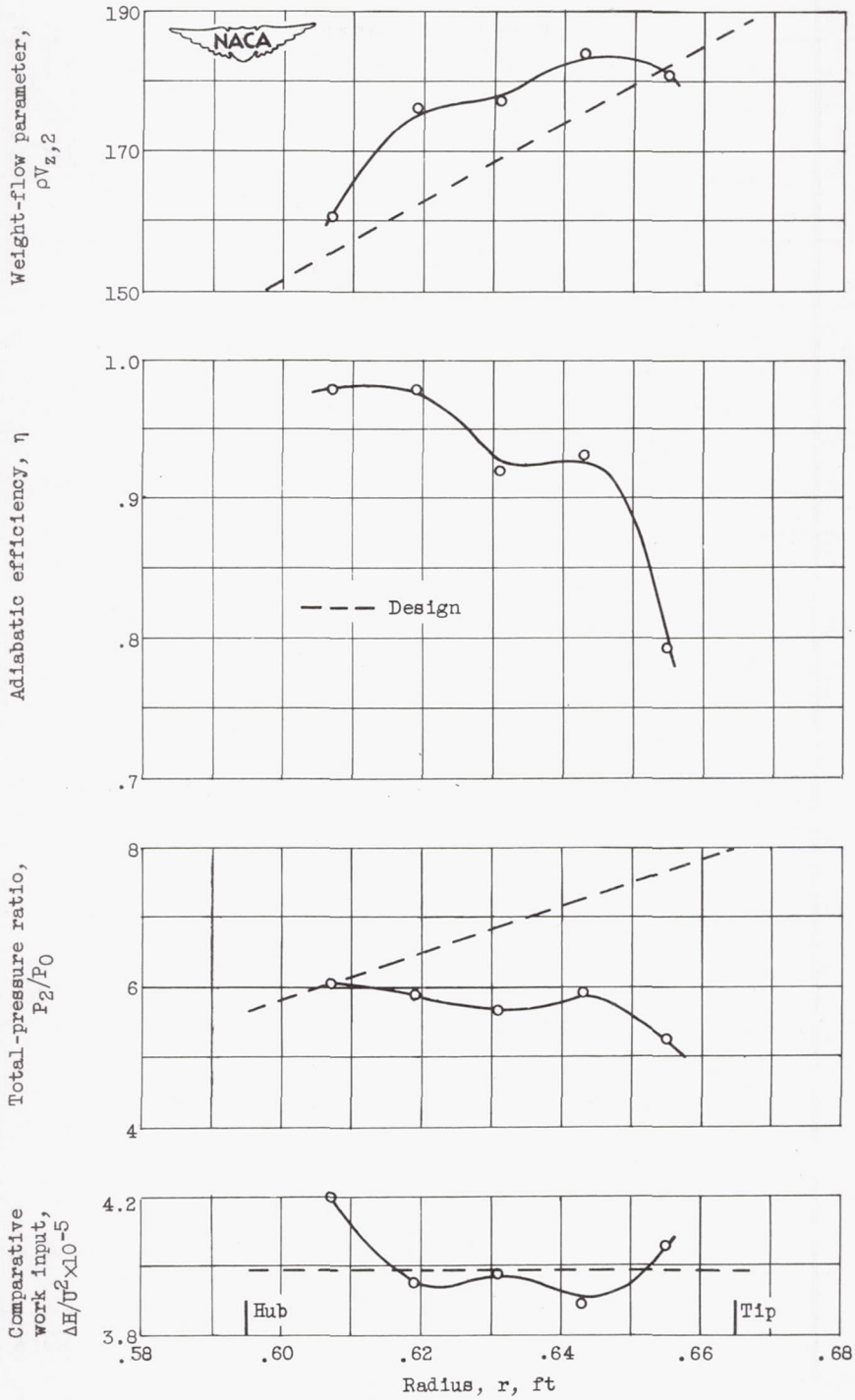


(a) Weight flow, efficiency, total-pressure ratio, and work input.

Figure 14. - Discharge conditions at 97.5-percent design speed and impulse operation (open throttle) for 16-inch impulse-type supersonic-compressor rotor with turning to axial direction.

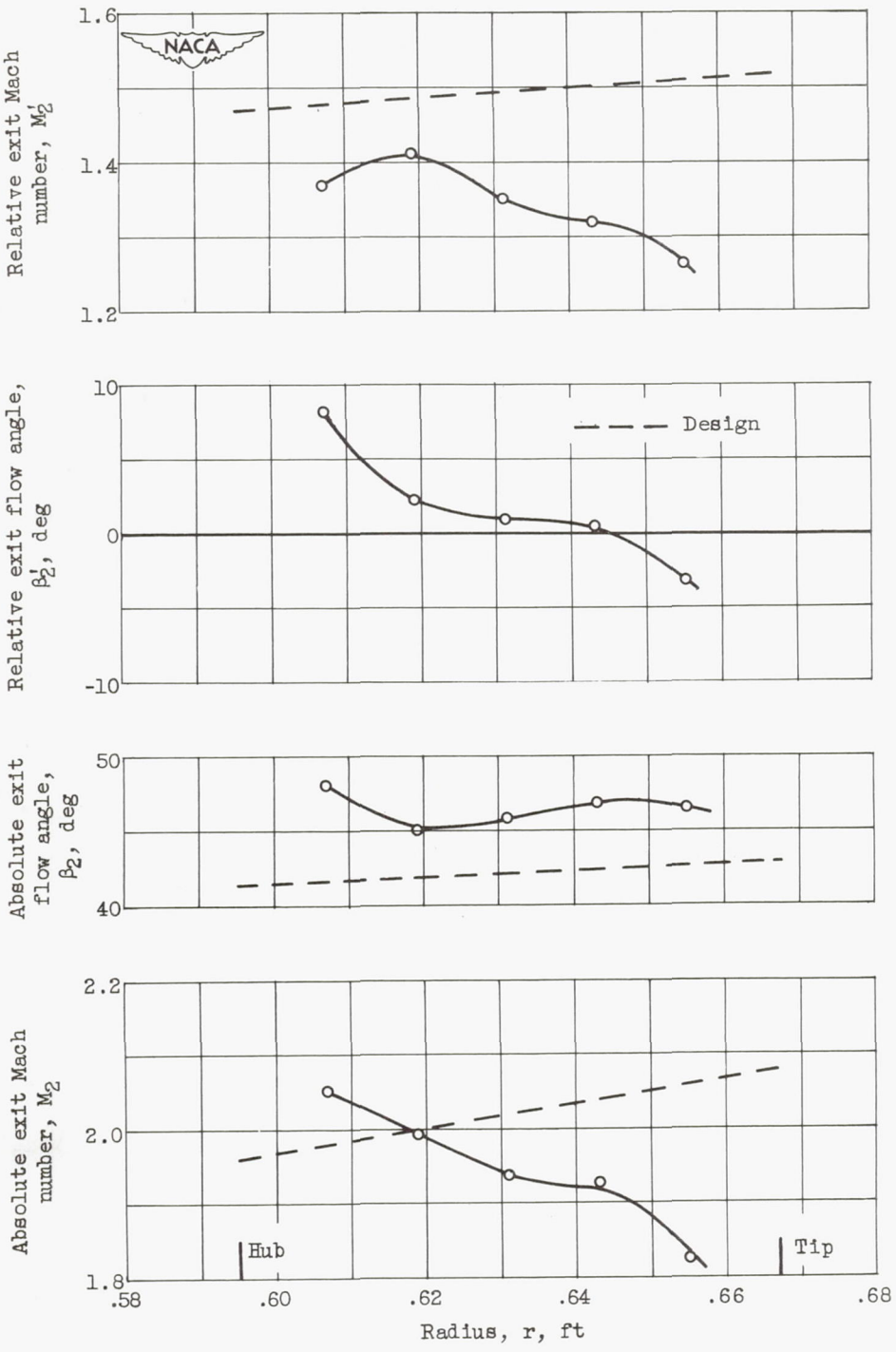


(b) Absolute and relative Mach numbers and flow angles.

Figure 14. - Concluded. Discharge conditions at 97.5-percent design speed and impulse operation (open throttle) for 16-inch impulse-type supersonic-compressor rotor with turning to axial direction.



NACA-Langley - 8-19-53 - 325

[redacted] INFORMATION

[redacted] CLASSIFIED

[redacted]